Macromolecules

Article

pubs.acs.org/Macromolecules

Terms of Use

# Monte Carlo Simulations of Multigraft Homopolymers in Good Solvent

Daniel G. Angelescu[†,*] and Per Linse[‡]

[†]Romanian Academy, "Ilie Murgulescu" Institute of Physical Chemistry, Splaiul Independentei 202, 060021 Bucharest, Romania

[‡]Physical Chemistry, Lund University, Box 124, SE-221 00 Lund, Sweden

Supporting Information

**ABSTRACT:** Multigraft polymers comprise a subclass of branched polymers where more than one side chain is attached to each node (branching point) of the main chain. We have investigated structural properties of single multigraft polymers under good solvent conditions by Monte Carlo simulations, employing a flexible bead−spring model. Beside the grafting density, denoting the linear density of grafted side chains, we have introduced the concept of branching density, denoting the linear density of nodes. At high branching density, both the branching density and the branching multiplicity controlled the structure of the side chains, whereas at lower branching density only the branching multiplicity influenced the side-chain structure. The spatial extension of the main chain and side chains as a function of side-chain length and grafting density was analyzed using scaling formalism. The dependence of the main-chain extension on side-chain length, branching density, and branching multiplicity could be collapsed on a universal curve upon relevant rescaling. Multigraft polymers with equal number of side-chain beads but unequal numbers and lengths of side chains displayed unconventional bending properties. Few and long side chains gave rise to a still relative low locally stiffness but considerable long-range rigidity, whereas more numerous and shorter side chains lead to a higher local stiffness but to a smaller long-range rigidity.

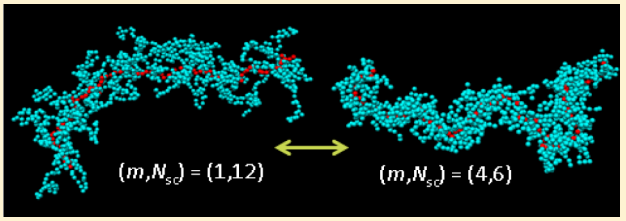


## 1. INTRODUCTION

A large class of branched polymers possesses two main structural elements: a main chain (also referred to as a backbone) and side chains that are chemically attached (end-grafted) to the main chain. The side chains are attached to nodes (branching points or junction points) located in the main chain. These branched polymers are typically referred to as (i) comb polymers when topologically neighboring nodes are well-separated appearing at low linear grafting density and (ii) bottle-brush polymers when topologically neighboring nodes are near each other appearing at high linear grafting density. Branched polymers have attracted considerable attention over the past decade from theoretical to applied research viewpoints because of the availability of many structural variables, which in turn may facilitate a design of new functional materials.[1,2]

The large conformational freedom of comb polymers leads to the existence of a rich variety of spatial structures that are controlled by, e.g., main-chain length, side-chain length, grafting density, chemical composition, and solvent quality.[3−5] As an example, thermoplastic elastomers or impact resistant materials could be obtained by tailoring the flexibility of the main chain and side chains.[6] Moreover, amphiphilic comb copolymers may find applications as hydrogels, surface modifying agents, dispersants, and transfection efficiency enhancer for gene delivery.[7] Designing such complex molecules for targeted applications represent a great challenge, as many parameters have to be taken into account for elucidating the structure−property relationship. One reason for this difficulty is the multitude of length scales, by which the conformation is characterized.[8] In view of these challenges, systematic simulations studies, including both on-lattice and off-lattice methods, have been carried out to investigate the conformational properties of comb polymers.[9−17] Two aspects were mostly investigated: conformation and scaling description of (i) the main chain and (ii) the side chains under various conditions concerning chain length, chain flexibility, grafting density, and solvent quality.

Whereas a limited number of studies have considered the dependence of the comb polymer conformation on the grafting density,[9,13,17] a larger number of computational studies have focused on properties of bottle-brush polymers at different side-chain grafting density.[8,11,13,15,18−21] Various conformations were predicted for flexible side chains attached to semiflexible or stiff main chains in the bottle-brush limit. The grafted chains underwent a transition from a near three-dimensional self-avoiding random walk (SAW)[17] to a near two-dimensional SAW.[9,18,22,23] Detailed discussion of the scaling concepts of bottle-brush polymers with semiflexible or rigid main chains revealed that the stretching in the radial direction depended on the number of side-chain beads $N_{sc}$ as $\sim N_{sc}^{3/5}$ in the former case,[11,12] whereas a $N_{sc}^{3/4}$ dependence was found in the latter case.[13,24]

**Received:** October 15, 2013
**Revised:** December 3, 2013
**Published:** December 24, 2013

 © 2013 American Chemical Society  dx.doi.org/10.1021/ma4021246 | *Macromolecules* 2014, 47, 415−426

The effect of the excluded volume interaction among side chains on the main-chain conformation in bottle-brush polymers is another important aspect investigated. Such studies have employed a semiflexible main-chain with flexible,[21] semiflexible,[8,11,13,15,18−20] or rigid[25] side chains. A stiffening of a flexible main chain was observed by increasing grafting density or length of side chains.[4,5,15,16] The systematic main-chain stiffening with increasing side-chain length was also reflected by a power-law behavior of the main-chain extension.[11,13,15] Although the simulation studies all agreed on the main-chain stiffening, discrepancies were found in the degree of stiffening: from a weak[8,9,15,18,21] to a strong[11,24] impact on the persistence length. Notably, the simulations revealed that the internal structure of a polymer with a topological stiffness is quite different from a flexible wormlike chain,[11] and caution is needed to extract a meaningful estimate of the persistence length as the definition of the persistence length is not unique and different ways of calculating it were considered.[19]

Yet another possibility to tailor properties of branched polymers is to change the functionality of the main-chain nodes. Polymers with multifunctional nodes, i.e., nodes to which more than one linear side chain is attached, are referred to as *multigraft* polymers. The multigraft concept has been exploited, and considerable progress have recently been achieved in the synthesis of multigraft polymers.[26−31] Synthesize of multigraft copolymers with tetrafunctional and hexafunctional nodes and with good control over the placement of the nodes has been demonstrated.[30]

To the best of our knowledge, such multigraft polymers have not yet been investigated by simulations. The present work intends to reduce this gap by exploring the structure of such branched polymers. Here, we pose mainly two questions: How do the properties of branched polymers depend on increasing node functionality under the condition of (A) *constant length of individual side chains* and (B) *constant mass of side chains attached to one node*? Answers to these questions were obtained by using a coarse-grained model solved by Monte Carlo simulations, from which equilibrium conformations of single multigraft polymers with flexible main and side chains under good solvent conditions were extracted. From the answers, two principle outcomes have arisen: (i) We need to discriminate between the *branching* density denoting the linear density of nodes to which side chains are attached and the *grafting* density denoting the linear density of grafted side chains. These two quantities are not equal for multigraft polymers. (ii) The spatial extension of side chains is controlled by both the omnipresent repulsion among side chains attached to the *same* node and from a branching-density dependent repulsion among side chains attached to *different* nodes, whereas the extension of the main chain at our conditions depended only on the number of grafted side chains.

## 2. MODEL AND METHOD

**2.1. Model.** We adopt a coarse-grained model extensively employed for simulations of polymers in solutions to examine the structural properties of flexible multigraft homopolymers under good solvent conditions. In this model, the polymer is represented by spherical beads that are joined in a branched topology. The beads are connected by harmonic bonds, and the flexibility of both main chain and side chains could be regulated by harmonic angular energy terms. We consider polymers with tri-, tetra-, and hexafunctional nodes, which in the literature are referred to as comb, centipede, and barbwire polymers, respectively.[31−33]

The branched topology investigated in this work is illustrated in Figure 1. The main chain is composed of $N_{mc}$ beads, which

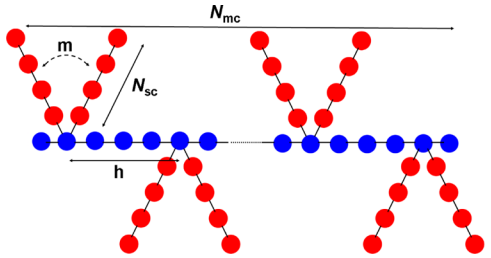


**Figure 1.** Schematic representation of the topology of a branched polymer possessing main-chain (blue) and side chain (red) beads, where $N_{mc}$ is number of main-chain beads, $h$ the bead increment between subsequent nodes, $N_{sc}$ the number of beads in one side chain, and $m$ the branching multiplicity. The second and the second last bead of the main chain are always nodes. Here, $h = 4$, $N_{sc} = 4$, and $m = 2$.

possesses $n_n$ nodes. Each node has $m$ side chains with $m = 1$, 2, or 4 for comb, centipede, or barbwire polymers, respectively. All nodes of a polymer have the same functionality. The second and second last bead of the main chain are always a node, and the remaining nodes are evenly distributed along the main chain, giving $n_n = (N_{mc} - 3)/h + 1$ nodes with $h$ being the increment of beads between subsequent nodes along the main chain. The number of side chains becomes $n_{sc} = mn_n$ and the total number of beads of a polymer $N = N_{mc} + n_{sc}N_{sc}$ with $N_{sc}$ denoting the number of beads in a side chain. Note, we will discriminate between (i) *branching* density and (ii) *grafting* density; the former is the fraction of nodes being branched, and the latter is the average number of grafted side chains per main-chain bead. Hence, the *branching* density becomes $\sigma_b = 1/h$ and the *grafting* density $\sigma_g = m\sigma_b \geq \sigma_b$. In the limit of monofunctional nodes, the two concepts branching density and grafting density coincide.

The total energy of the polymer system is given as a sum of three terms according to

$$U = U_{nonbond} + U_{bond} + U_{angle} \tag{1}$$

The nonbonding term $U_{nonbond}$ is assumed to be pairwise additive and given by

$$U_{nonbond} = \sum_{i<j}^{N} u_{ij}(r_{ij}) \tag{2}$$

where $u_{ij}$ is the interaction between bead $i$ and $j$ separated by the distance $r_{ij}$ and the sum runs over all pair of beads of the branched polymer. A soft repulsive interacting potential between *all* beads is established by using the truncated and shifted Lennard-Jones (LJ) potential according to

$$ui_j(r_{ij}) = \begin{cases} 4\varepsilon\left[-\left(\frac{\sigma}{r_{ij}}\right)^6 + \left(\frac{\sigma}{r_{ij}}\right)^{12} + \frac{1}{4}\right], & r_{ij} \leq 2^{1/6}\sigma \\ 0, & r_{ij} > 2^{1/6}\sigma \end{cases} \tag{3}$$

where $\sigma$ is the bead diameter and $\varepsilon$ the bead−bead interaction strength. The bond energy $U_{bond}$ entering in eq 1 is given by

$$U_{bond} = \sum_{i<j}^{N} \frac{k_{bond}}{2}(r_{ij} - r_0)^2\Omega_{ij} \tag{4}$$


dx.doi.org/10.1021/ma4021246 | Macromolecules 2014, 47, 415−426

where $\Omega_{ij} = 1$ for bead $i$ and $j$ bonded to each other, otherwise 0, $r_0$ is the equilibrium bond distance ($r_0$ = 5 Å), and $k_{bond}$ is the bond force constant ($k_{bond}$ = 0.4 N m$^{-1}$). The bond–bond angular potential energy $U_{angle}$ of eq 1 is represented by

$$U_{angle} = \sum_{i=2}^{N-1} \frac{k_{angle}}{2}(\alpha_i - \alpha_0)\Omega_{i-1,i,i+1} \quad (5)$$

where $\alpha_i$ is the angle between the position vectors $\mathbf{r}_{i+1} - \mathbf{r}_i$ and $\mathbf{r}_{i-1} - \mathbf{r}_i$ with $\Omega_{i-1,i,i+1} = 1$ if bead $i - 1$, $i$, and $i + 1$ are located in the main chain or in the same side chain, otherwise 0, $\alpha_0$ is the equilibrium angle ($\alpha_0$ = 180°), and $k_{angle}$ is the angular force constant. In this work, $k_{angle} = 0.51 \times 10^{-24}$ J deg$^{-2}$ was used giving a persistence length of $l_p^0$ = 7.8 Å of a linear chain, as evaluated according to the relation[34]

$$l_p = R_{BB}/(1 + \cos\langle\alpha\rangle) \quad (6)$$

with $R_{BB} \equiv \langle R_{BB}^2\rangle^{1/2}$ denoting the root-mean-square (rms) bead–bead separation. The small value of $k_{angle}$ affected the persistence length only marginally, and hence the main chain was classified as being flexible. The parameters of the polymer model are summarized in Table 1.

**Table 1. Parameters and their Values Describing the Branched Polymer**

| | |
|---|---|
| number of beads in the main chain[a] | $N_{mc}$ = 99 |
| number of nodes in the main chain[b] | $n_n$ = 3–49 |
| bead increment between adjacent nodes[b] | $h$ = 2–48 |
| branching density[b] | $\sigma_b$ = 0.0208–0.5 |
| branching multiplicity | $m$ = 1, 2, and 4 |
| number of beads in one side chain | $N_{sc}$ = 6–24 |
| bead–bead size LJ parameter | $\sigma$ = 3.405 Å |
| bead–bead energy LJ parameter | $\varepsilon$ = 0.9961 kJ mol$^{-1}$ |
| equilibrium separation of bond potential | $r_{eq}$ = 5.0 Å |
| force constant of bond potential | $k_{bond}$ = 0.4 N m$^{-1}$ |
| equilibrium angle of angle potential | $\alpha_0$ = 180° |
| force constant of angular potential | $k_{angle} = 0.51 \times 10^{-24}$ J deg$^{-2}$ |

[a]Some simulations with $N_{mc}$ = 339 main-chain beads have been performed to examine main-chain length dependences. [b]Only one of these three properties are independent.

**2.2. Systems Considered.** We have studied single polymers having a main chain with $N_{mc}$ = 99 beads and side chains possessing from $N_{sc}$ = 6 to 24 beads each. Furthermore, the number of nodes $n_n$ ranged from 3 to 49, leading to a variation of the bead increment between grafted nodes and the branching density ($h$, $\sigma_b$) from (48, 1/48 ≈ 0.0208) to (2, 1/2).

Central to our study is the effect of having multiple side chains grafted to one node. Our aim is to answer the questions:

(A) How does the branching multiplicity at *constant length of individual side chains*, and hence at varying number of side-chain beads per node (Figure 2a), affect polymer properties?

(B) How does the branching multiplicity at *constant number of side-chain beads associated with a node*, and hence at varying side-chain length (Figure 2b), affect polymer properties?

**2.3. Simulation Details.** Structural properties of the model system were obtained by performing Metropolis Monte Carlo (MC) simulations in the canonical ensemble. One branched polymer was placed within a cubic simulation box, whose length was $L$ = 300 Å, and the temperature $T$ = 298 K was employed. Periodic boundary conditions were applied in all three directions.

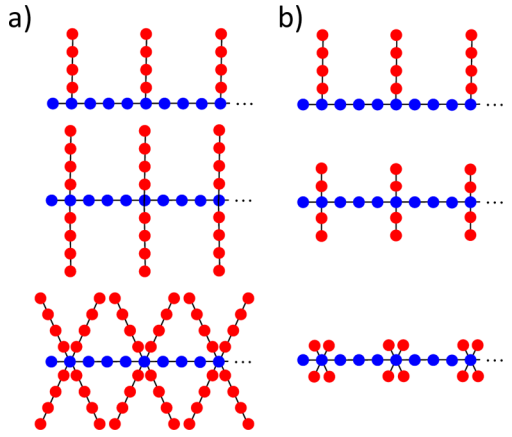


**Figure 2.** Schematic illustration of the main chain (blue circles) with varying distribution of side chains (red circles) along it. (a) Increasing branching multiplicity at *fixed side-chain length* by increasing the number side-chain beads (top to bottom) and (b) increasing branching multiplicity at *fixed number of side-chain beads* by decreasing side-chain length (top to bottom).

The branched polymer was subjected to two kinds of trial displacements: (i) single-bead translational move and (ii) pivot rotation of a randomly selected part of the polymer. In the latter case, a bead of the branched polymer was selected randomly. If the bead resided in the main chain, the shorter part of the main chain and the side chains attached to that part were selected for a trial rotation. If the bead resided in a side chain, the nongrafted part of the side chain was subjected to the trial rotation.

After equilibration involving $5 \times 10^4$ passes (attempted moves per particle), the production runs comprised typically $5 \times 10^5$ passes. The reported uncertainties were calculated by dividing the total simulation in 5 sub-batches, and they are presented as one standard deviation of the mean. Note, the reported uncertainties in figures are in most cases smaller than the symbol size, and in these cases they are invisible.

We have in some cases examined the ergodicity of our systems by performing simulations from different initial conformations. In all these cases, the spread of mean values between simulations of same systems were within the precision obtained for the individual simulations.

All simulations were performed using the integrated Monte Carlo/molecular dynamics/Brownian dynamics simulation package MOLSIM.[35]

**2.4. Structural Characterization.** The structures of the branched polymers were characterized by the following quantities:

1. Rms radius of gyration of the main chain $R_{G,mc}$, of the side chain $R_{G,sc}$, and of the branched polymer $R_G$ defined as

$$R_G \equiv \langle R_G^2\rangle^{1/2} = \frac{1}{M}\langle \sum_{i=1}^{M} |\mathbf{r}_i - \mathbf{r}_{com}|^2\rangle \quad (7)$$

where $M$ is the number of beads, i.e., $M = N_{mc}$, $M = N_{sc}$, and $M = N$, respectively, $\mathbf{r}_i$ is the position vector of bead $i$, and $\mathbf{r}_{com}$ the location of the center of mass of the main chain, of the side chain, and of the branched polymer, respectively. As to $R_{G,sc}$, $\langle ... \rangle$ also imply an average over all side chains.

2. Rms end-to-end distance of the main chain $R_{EE,mc}$ and of side chains $R_{EE,sc}$ according to

$$R_{EE} \equiv \langle R_{EE}^2\rangle^{1/2} = \langle |\mathbf{r}_1 - \mathbf{r}_M|^2\rangle^{1/2} \quad (8)$$


dx.doi.org/10.1021/ma4021246 | Macromolecules 2014, 47, 415–426

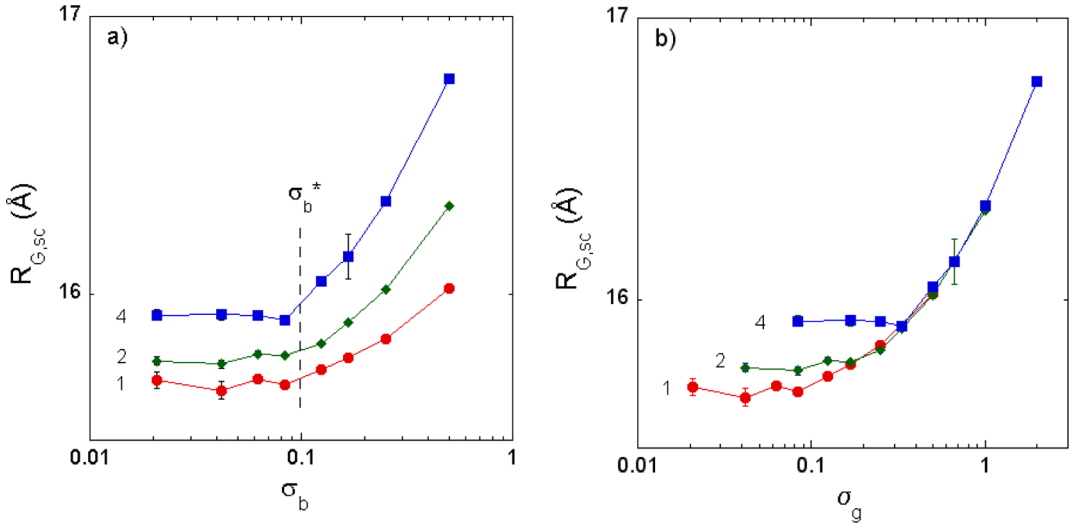


**Figure 3.** (a) Rms radius of gyration of side chains $R_{G,sc}$ as a function (a) of the branching density $\sigma_b$ and (b) of the grafting density $\sigma_g$ in a log–log representation for side-chain length $N_{sc} = 24$ and branching multiplicity $m = 1$ (●), $m = 2$ (◆), and $m = 4$ (■).

where $\mathbf{r}_1$ and $\mathbf{r}_M$ are positions of the first and the last bead of the main chain ($r_M = r_{N_{mc}}$) and of the side chain ($r_M = r_{N_{sc}}$), respectively. As to $R_{EE,sc}$, $\langle ... \rangle$ also imply an average over all side chains. The qualitative features of $R_G$ and $R_{EE}$ turned out to be the same, and therefore the results of the latter are given as Supporting Information.

3. Scaling relation describing how the rms radius of gyration $R_G$ and the rms end-to-end distance $R_{EE}$ of the main chain, side chains, or polymer depend on the number of beads in a side chain $N_{sc}$ and on the branching density $\sigma_b$ according to

$$R_{Xy} \sim N_{SC}^{\nu} \tag{9}$$

and

$$R_{Xy} \sim \sigma_b^{\mu} \tag{10}$$

with X either G or EE and y either mc, sc, or missing for the polymer.

4. Asphericity of the main chain $A_{mc}$ and of the branched polymer $A$ defined as

$$A = \left\langle \frac{(E_1 - E_2)^2 + (E_2 - E_3)^2 + (E_3 - E_1)^2}{2(E_1 + E_2 + E_3)^2} \right\rangle \tag{11}$$

where $E_1$, $E_2$, and $E_3$ are the eigenvalues of the moment of inertia tensor $\mathbf{E}$ with the elements

$$\mathbf{E}_{\alpha\beta} = \sum_{i}^{M} (\mathbf{r}_{\alpha,i} - \mathbf{r}_{\alpha,com})(\mathbf{r}_{\beta,i} - \mathbf{r}_{\beta,com}),$$
$$(\alpha, \beta) = (x, y, z) \tag{12}$$

with $M$ being the number of beads, i.e., $M = N_{mc}$ and $M = N$, respectively. The asphericity ranges from 0 (sphere) to 1 (rod).

5. Form factor of the main chain $F_{mc}(q)$ and of the branched polymer $F(q)$ defined according to

$$F(q) = \frac{1}{M}\langle |\sum_{i,j=1}^{M} \exp(i\mathbf{q}\cdot\mathbf{r}_{ij})|^2 \rangle \tag{13}$$

where $M$ is the number of beads, i.e., $M = N_{mc}$ and $M = N$, respectively, $q = |\mathbf{q}|$ the wavenumber, and $\mathbf{r}_{ij}$ the vector between the coordinates of bead $i$ and $j$.

## 3. RESULTS

First, we consider the scaling behavior of linear polymers possessing $N$ beads, where the polymers are described by relevant parameters in Table 1. The rms radius of gyration $R_G$ for $100 < N < 300$ satisfied the scaling relation $R_G \sim N^{\nu}$ with $\nu = 0.59$, consistent with the scaling behavior under good solvent conditions, $\nu \approx 0.588$.[36] As the branched architectures considered here involved shorter side chains, the scaling of linear chains for $6 \leq N \leq 24$ was also examined. For these shorter chains, we obtained $\nu = 0.64$.

**3.1. Fixed Side-Chain Length.** Our first question deals with how properties of a branched and flexible polymer are affected by the branching multiplicity at fixed side-chain length and how the branching density potentially influences the answer (see Figure 2a). We consider properties of (i) side chains, (ii) the main chain, and (iii) the polymer separately.

*3.1.1. Properties of the Side Chains.* Figure 3a displays the rms radius of gyration of the side chains $R_{G,sc}$ as a function of the branching density $\sigma_b$ with the longest side chain $N_{sc} = 24$ at different values of the branching multiplicity $m$. Corresponding data for the end-to-end distance of side chains $R_{EE,sc}$ are given in Figure S1a, Supporting Information. The principle feature is an appearance of two regimes with a crossover at $\sigma_b = \sigma_b^* \approx 0.1$. Below the crossover, the extension of the side chains is independent of the branching density and increases with increasing branching multiplicity. Above the crossover, the extension of the side chains increases with increasing branching density and it still increases with increasing branching multiplicity. The value of the crossover branching density $\sigma_b^* \approx 0.1$ is similar for $R_{G,sc}$ and $R_{EE,sc}$ and independent of the branching multiplicity.

In Figure 3b and Figure S1b, same data but as a function of the grafting density $\sigma_g$, instead of the branching density $\sigma_b$, are given. In this representation, at high $\sigma_g$ the curves collapse onto a master curve, demonstrating that the extension of the side chains depends rather on the number of grafted side chains than on the distribution of them along the main chain. Noticeable, with $\sigma_g$ as abscissa the previously common crossover has vanished; instead the leveling off at reduced $\sigma_g$ appears at different values of $\sigma_g$ that depends on the branching multiplicitiy.


dx.doi.org/10.1021/ma4021246 | Macromolecules 2014, 47, 415–426

Side chains near main-chain ends are expected to display a somewhat smaller extension than other side chains due to a larger space available. The selected simulations with a longer main chain possessing $N_{mc}$ = 339 beads gave same results as for $N_{mc}$ = 99. Thus, we conclude that main-chain end-effects on the averaged side-chain data are here negligible for the systems with $N_{mc}$ = 99 main-chain beads.

As to the side-chain end-to-end distance, in the bottle-brush limit (high $\sigma_b$) the increase of the end-to-end distance $R_{EE,sc}$ with $\sigma_b$ followed a power dependence according to $R_{EE,sc} \sim \sigma_b^{\mu_{sc}}$ with $\mu_{sc}$ ranging from 0.03 for $m$ = 1 to 0.06 for $m$ = 4. The values of $\mu_{sc}$ are smaller than those predicted for strongly overlapping side chains. Computer simulations using bond-fluctuation model of polymers gave an exponent of 0.1,[13] whereas a mean-field prediction gave 0.12.[37]

We now analyze the extension of the side chains as a function of the number of beads in the side chains according to $R_{G,sc} \sim N_{sc}^{\nu_{sc}}$ and $R_{EE,sc} \sim N_{sc}^{\nu_{sc}}$ with $\nu_{sc}$ being a fitting parameter. Figure 4

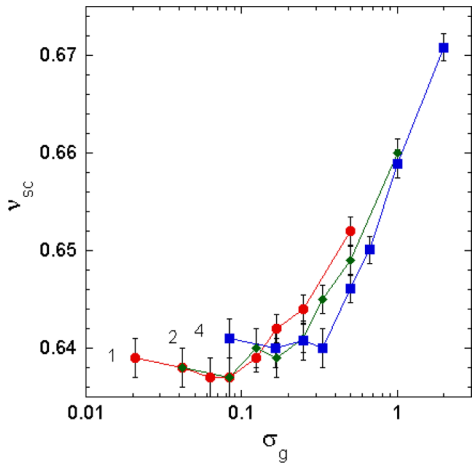


**Figure 4.** Exponent $\nu_{sc}$ as fitted from $R_{G,sc} \sim N_{sc}^{\nu_{sc}}$ as a function of the grafting density $\sigma_g$ in a log-lin representation for branching multiplicity $m$ = 1 (●), $m$ = 2 (◆), and $m$ = 4 (■).

and Figure S2 show the fitted $\nu_{sc}$ as a function of the *grafting* density $\sigma_g$ with the branching multiplicity $m$ as a parameter for the two spatial extension properties. Not unexpectedly, also $\nu_{sc}(\sigma_g)$ exhibit two regimes with a crossover; however, with $\sigma_g$ as abscissa the crossover becomes $m$-dependent. At grafting densities $\sigma_g < m\sigma_b^*$, $m$ = 1 and 2, $\nu_{sc}$ is basically independent of $\sigma_g$ with $\nu_{sc}$ being larger than that of a free polymer of same length, but for the branching multiplicity $m$ = 4 $\nu_{sc}$ becomes considerably larger. At grafting densities $\sigma_g > 0.5$, (i) $\nu_{sc}$ increases strongly and (ii) its dependence on $m$ is reduced at increasing grafting density.

From these observations, we conclude that at low branching density ($\sigma_b < \sigma_b^*$) side chains attached to adjacent nodes are still too far away to affect each other's spatial extension. However, noticeable excluded-volume interaction appears among side chains attached to the *same* node, which affects the main-chain scaling property (see subsection 3.1.2). In the regime of high branching density ($\sigma_b > \sigma_b^*$), side chains attached to adjacent nodes experience mutual repulsion, in addition to the repulsive interaction with side chains attached to the same node. The increased value of $m\sigma_b^*$ at increasing $m$ is a consequence that beads located in side chains attached to adjacent nodes start to effectively repel each other at a node−node separation insensitive of $m$.

It should be mentioned that $\nu_{sc}$ potentially is depended on the main-chain and side-chain lengths. Side chains located at the distance $d \sim N_{sc}^{\nu_{sc}}$ or shorter from a main-chain end are expected to be less compressed as compared to those further away from an end. Hence, the end effects become relatively less important at increasing $N_{mc}$ and decreasing $N_{sc}$. With $N_{sc} \leq 50$, a saturation for $N_{mc} > 250$ have been reported.[15] These results imply that the salient features exhibited by our multigraft polymer model with $N_{sc} \leq 24$ most likely could be assessed with $N_{mc}$ = 99. We notice that at the highest branching density $\sigma_b$ = 0.5, the value of $\nu_{sc}$ for singly grafted chains is comparable to previously reported simulation data[11,12,15,38,39] and experimental results.[40−42]

The representation of the side chains of bottle-brush polymers using the Daoud−Cotton blob picture to model the excluded-volume pressure exerted from adjacent grafted side chains provided the theoretical predictions $\nu_{sc}$ = 3/4.[37,43] Other experimental and computer simulations results[13,44] predict $\nu_{sc} \geq 0.7$. Thus, our exponent at large grafting density is comparable to, but slightly smaller than, theoretical values.

*3.1.2. Properties of the Main Chain.* The extension of the main chain was analyzed in a similar fashion as of the side chains. The radius of gyration of the main chain $R_{G,mc}$ as a function of the branching density $\sigma_b$ with the longest side chain $N_{sc}$ = 24 at $m$ = 1, 2, and 4 is shown in Figure 5a. In contrast to $R_{G,sc}$, $R_{G,mc}$ increases

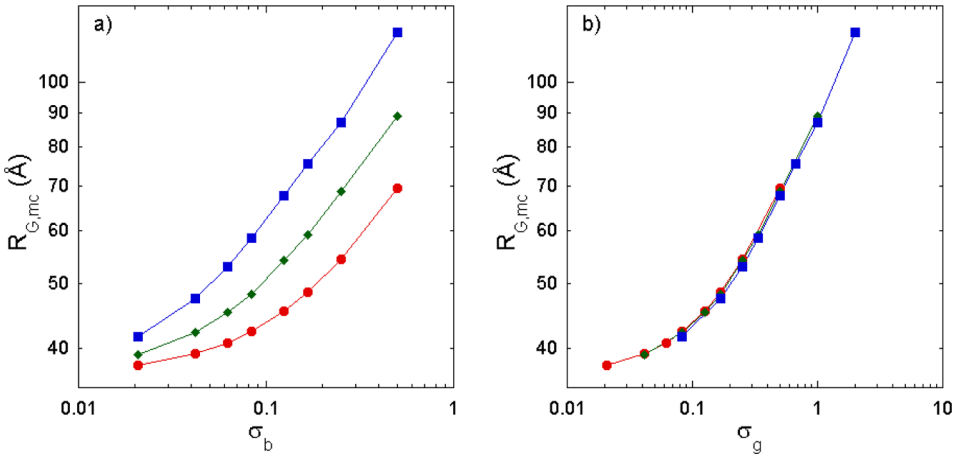


**Figure 5.** (a) Radius of gyration of main chain $R_{G,mc}$ as a function (a) of the branching density $\sigma_b$ and (b) of the grafting density $\sigma_g$ in a log−log representation for side-chain length $N_{sc}$ = 24 and branching multiplicity $m$ = 1 (●), $m$ = 2 (◆), and $m$ = 4 (■).


dx.doi.org/10.1021/ma4021246 | Macromolecules 2014, 47, 415−426

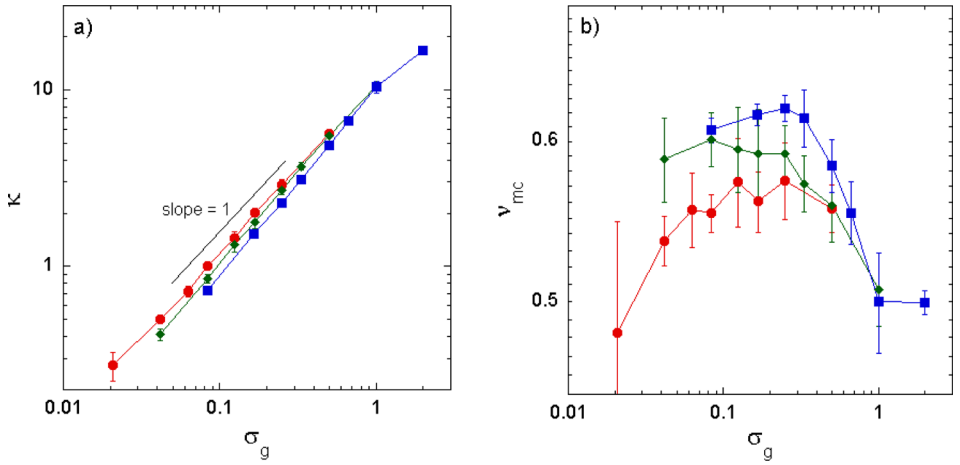


**Figure 6.** (a) Pre-exponential factor $\kappa$ and (b) the exponential factor $\nu_{mc}$ as a function of the grafting density $\sigma_g$ in a log−log representation for branching multiplicity $m$ = 1 (●), $m$ = 2 (◆), and $m$ = 4 (■).

continuously with increasing branching density, whereas, as $R_{G,sc}$, $R_{G,mc}$ increases with increasing multiplicity at constant $\sigma_b$. However, when viewing $R_{G,mc}$ as a function of the grafting density $\sigma_g$, Figure 5b displays a complete collapse over the full range of $\sigma_g$. Hence, the main-chain extension is determined, in addition to the side-chain length, also on the number of attached side-chains but *not* on their distribution in terms of multigraft up to $m$ = 4. Remember, that in our study all nodes of the main-chain are spanning the full main-chain length with equal separation.

As to the $N_{sc}$-dependence, we mention that in contrast to the side chains, the main chain have a nonzero extension at $N_{sc} = 0$. In the following, we assume the reasonable functional form of $R_{G,mc}(N_{sc})$ according to

$$R_{G,mc}(N_{sc}) = R_{G,mc}(N_{sc} = 0) + \kappa N_{sc}^{\nu_{mc}} \quad (14)$$

where the first term on the rhs denotes the rms radius of gyration of an ungrafted main chain and the second term the influence of the grafted side chains on the radius of gyration of the main chain. In the second term, the prefactor $\kappa$ and the exponent $\nu_{mc}$ are dependent on the branching density $\sigma_b$ (alternatively the grafting density $\sigma_g$) and the branching multiplicity $m$. Figures 6a and 6b show the extracted $\kappa$ and $\nu_{mc}$, respectively, for all three branching multiplicities as a function of $\sigma_g$, whereas Figure S3a shows underlaying least-squares fits to eq 14 for the three branching multiplicities and three densities. The rms end-to-end distance of the main chain has been analyzed using an equation analogous to eq 14. The fitted $\kappa$ and $\nu_{mc}$ as a function of $\sigma_g$ are provided in Figure S4, and Figure S3b shows the actual fit for, again, three grafting densities. Below, equations and data for $R_{EE,mc}$ will be given in parentheses

The least-square fits yielded prefactors $\kappa \sim \sigma_g$ ($\kappa \sim \sigma_g^{0.9}$) at all branching multiplicities according to Figure 6a (Figure S4a), and the exponent $\nu_{mc}$ varied less regularly with the grafting density $\sigma_g$ and the branching multiplicity $m$—see Figure 6b (Figure S4b). For the intermediate grafting density $0.1 < \sigma_g < 0.6$, $\nu_{mc}$ is basically $\sigma_g$ independent and its value increases from $\nu_{mc}$ = 0.57 (0.60) at $m$ = 1 to $\nu_{mc}$ = 0.62 (0.65) at $m$ = 4. The value of $\nu_{mc}$ decreases at grafting density lower than 0.1 for $m$ = 1 and 2 as well as at grafting density higher than 0.6 for $m$ = 2 and 4.

At grafting densities $\sigma_g < \sigma_g^*$, the values $\nu_{mc}$ = 0.48−0.57 (0.53−0.60) are larger than 0.36 as theoretically predicted.[9,37,45] Other simulation studies of comb polymers provide scattered values of the scaling-law exponent of the main-chain extension as a function the length of the side chains.[9,11−13,15,18] Moreover, the simulations focused on branched polymers in the brush limit $\sigma_b$ = 0.5 and 1.0,[8,11,12,15,18] whereas the main-chain behavior at low and intermediate branching density was scarcely investigated.[9] Saariaho et al.[18] found that the main-chain rms radius of gyration of brushes increased with $N_{sc}$ as $R_{G,mc} \sim N_{sc}^{\nu_{mc}}$ with $\nu_{mc}$ = 0.54, as predicted theoretically.[9] On the other hand, for bottle-brushes Khalatur et al.[13] reported a power-law behavior with $\nu_{mc}$ = 0.39, a value rather predicted for low grafting density. Moreover, our scaling relationship $\kappa \sim \sigma_g$ ($\kappa \sim \sigma_g^{0.9}$) held also for the longer chain with $N_{mc}$ = 339 beads. At this stage, we conclude that the values obtained for a wide range of grafting densities are in reasonable agreement with the exponent $\nu_{mc}$ = 0.54 previously reported for the situation of densely grafted side chains.[9,12]

On the basis of the behavior of the parameters $\kappa$ and $\nu_{eff}$ describing the rms radius of gyration of the main chain displayed in Figure 6, we now consider $R_{G,mc}/R_{G,mc}(\sigma_g = 0)$ as a function of $\sigma_g N_{sc}^{\nu_{mc}}$. Here, $\nu_{mc}$ was approximated as being independent of the grafting density $\sigma_g$, and we used the mean values $\nu_{mc}$ = 0.57, 0.59, and 0.62 extracted from Figure 6b (0.60, 0.63, and 0.65 from Figure S4b) for $m$ = 1, 2, and 4, respectively. The rescaling leads to a near complete collapse of data into a master curve as displayed in Figure 7 (Figure S5). Moreover, the good overlap in Figure 7 supports our notion that our results are, if at all, only marginally subjected to chain-end effects. Such a master curve denoting the dependence of the main-chain extension on the grafting density and side-chain length has not earlier been given in the previous studies of comb polymers.[9,12,13,17,18]

*3.1.3. Properties of the Branched Polymer.* We will now consider properties of the branched polymer as one entity. Thus, no discrimination of contributions from the main- or side-chain beads to investigated property will be made.

Rms radius of gyration $R_G$ of the branched polymer as a function of the grafting density $\sigma_g$ at different branching multiplicity and at the three side-chain lengths $N_{sc}$ = 6, 12, and 24 are shown in Figure 8. We observe that $R_G$ is (i) an increasing function of $\sigma_g$, (ii) dependent on the side-chain length; larger extension for longer side chains, and (iii) affected by the branching multiplicity only at grafting densities $\sigma_g \leq 0.2$. Observation (i) illustrates that the side-chain repulsion significantly increases the overall polymer extension with increasing grafting density. Clearly, similar mechanism, but at increasing side-chain length, lies behind observation (ii). Observation (iii) is rationalized again by assuming that two


dx.doi.org/10.1021/ma4021246 | *Macromolecules* 2014, 47, 415−426

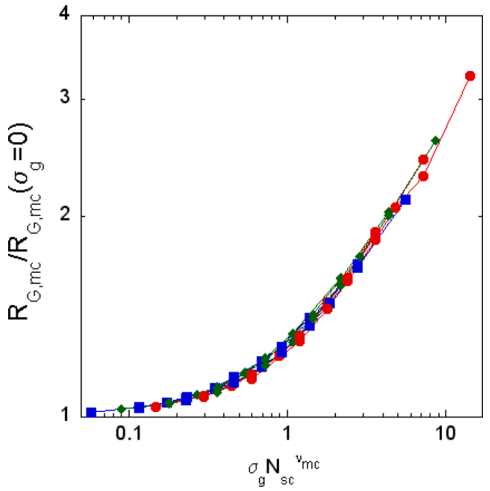


**Figure 7.** Normalized rms end-to-end distance of the main chain in a log−log representation as a function of $\sigma_g N_{sc}^{\nu_{mc}}$ for side-chain length $N_{sc}$ = 6 (■), $N_{sc}$ = 12 (♦), and $N_{sc}$ = 24 (●) and ($m$, $\nu_{mc}$) = (1, 0.57), (2, 0.59), and (4, 0.62).

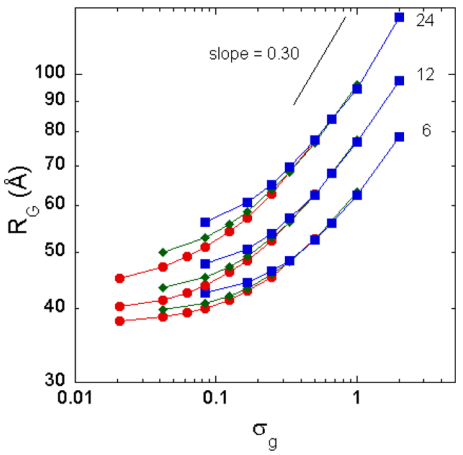


**Figure 8.** Radius of gyration of the branched polymer $R_G$ as a function of the grafting density $\sigma_g$ in a log−log representation for branching multiplicity $m$ = 1 (●), $m$ = 2 (♦), and $m$ = 4 (■) at indicated side-chain length $N_{sc}$.

side chains attached to *adjacent* nodes experience a similar mutual repulsion as two side chains attached to *same* nodes when the grafting density becomes sufficiently high; here, $\sigma_g > 0.2$. Hence, the realization of a given grafting density through a variation of branching density and multiplicity does not affect $R_G$ given a sufficient large grafting density. We propose that this appears as long as the characteristic side-chain length is longer than the characteristic node−node separation.

Although an exact scaling analysis of $R_G$ as a function of $\sigma_g$ according to $R_G \sim \sigma_g^{\mu}$ could not be performed, least-square fits performed on data at large values of $\sigma_g$ indicates that $R_G$ can be expressed by a power-law dependence, in analogy to what was done for side and main chains and in agreement with the scaling investigation of the overall flexible brush performed by Khalatur et al.[13] The best fit for $\sigma_g > 0.2$ gave $\mu = 0.30$, independent of the side-chain length. The value $\mu = 0.30$ is comparable to $\mu = 0.36$ for the scaling behavior of the radius of the gyration of the main chain $R_{G,mc}$ given in Figure S6. We notice a similar dependence of $\sigma_g$ for the branched polymer and the main chain. The obtained exponent for $R_{G,mc}$ is comparable to those predicted by the theory[37,45] and computational modeling[13] of branched polymers with densely grafted side chains, whereas the model predictions indicated a significant contribution of the side chains to the overall polymer extension.

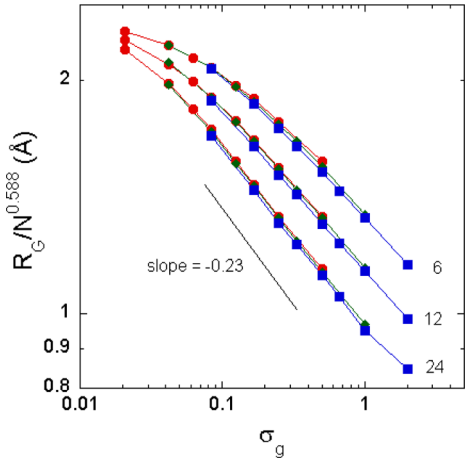


**Figure 9.** (a) Radius of gyration of the polymer normalized to the total number of beads $R_G/N^{0.588}$ as a function of the grafting density $\sigma_g$ in a log−log representation for branching multiplicity $m$ = 1 (●), $m$ = 2 (♦), and $m$ = 4 (■) at the indicated side-chain length $N_{sc}$.

Figure 9 displays $R_G$ normalized by $N^{0.588}$ with $N$ being the number of beads of the branched polymer vs grafting density $\sigma_g$. It is observed that the normalized $R_G$ (i) decreases with increasing grafting density $\sigma_g$, (ii) does not depend on the branching multiplicity $m$ provided constant $\sigma_g$, and (iii) exhibits a power law dependence on the overall number of side-chain beads $N_{sc}$ for $\sigma_g > 0.15$. The exponent varied with the side-chain length, from −0.20 for $N_{sc}$ = 6 to −0.23 for $N_{sc}$ = 24. These values of the exponent obtained for strongly overlapping side chains agree well with the theoretical and computational prediction of −0.24[37,45] and −0.23,[13] respectively, made for flexible brushes. The observations (i−iii) were also found for the systems with the longer main chain.

**3.2. Fixed Number of Side-Chain Beads.** Further aspects on the influences of the branching multiplicity on polymer properties will now be given. Those will be obtained by comparing properties of (i) *three* different combinations of branching multiplicity $m$ with the number of beads in a side chain $N_{sc}$, such that the number of beads associated with a node $mN_{sc}$ is *constant* (*cf.* Figure 2b) for (ii) *three* different branching densities $\sigma_b$. Hence, in total nine different systems.

*3.2.1. Snapshots.* Snapshots of equilibrium conformations of the nine systems are provided by Figure 10. We easily distinguish the main chain from the surrounding side chains. In particular, at the highest branching density side-chain beads form a compact brush region that we in the following will refer to as the *dress* of the main chain. Noticeably is that short side chains $N_{sc}$ = 6 (by necessity) are spatially close to the main chain, whereas the long ones $N_{sc}$ = 24 typically extend further away from the main chain. Moreover, we find that the sequence of increased multiplicity combined with shorter side chains, ($m$, $N_{sc}$) = (1, 24) → (2, 12) → (4, 6), leads to a change of the main-chain conformation. A central question is how the difference in the organization of a given number of side-chain beads, through their steric repulsion, affects the main-chain structure.

*3.2.2. Real-Space Characterization.* A more quantitative analysis will now follow. The persistence length and the


dx.doi.org/10.1021/ma4021246 | *Macromolecules* 2014, 47, 415−426

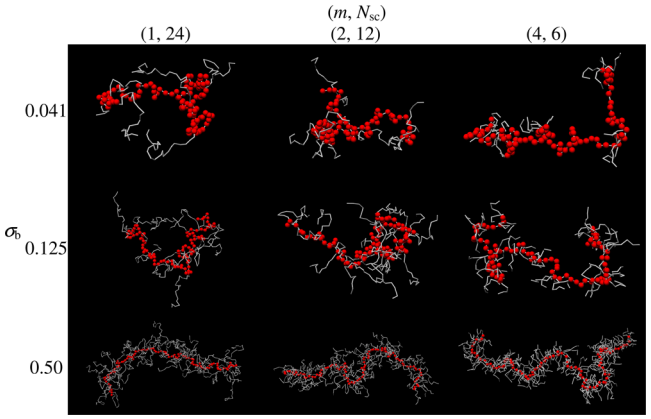


**Figure 10.** Snapshot of equilibrium configurations for branched polymers with $N_{mc}$ = 99 main-chain beads and $mN_{sc}$ = 24 side-chain beads associated with each node for indicated values of branching multiplicity $m$, side-chain length $N_{sc}$, and branching density $\sigma_b$. Main-chain beads are represented by red spheres and side chains by thin white lines. The scales vary across the panels.

asphericity $A$ of the main chain as well as the rms radius of gyration $R_G$ and the asphericity $A$ of the polymer, all as a function of branching density $\sigma_b$ with the value of $(m, N_{sc})$ as a parameter, are displayed in Figure 11. We recall that the number of beads associated with a node $mN_{sc}$ is held constant.

The main-chain persistence length $l_{p,mc}$ (Figure 11a), representing the local stiffness of the main chain, supports the notion of an increased stiffness at increasing branching density at a constant side-chain length. The increase of the persistence length is small at $\sigma_b \leq 0.02$ but substantial at $\sigma_b > 2$. Moreover, the short-range straightening of the main chain is clearly increased for the sequence $(m, N_{sc}) = (1, 24) \rightarrow (2, 12) \rightarrow (4, 6)$, during which the main-chain dress of side-chain beads becomes denser (see Figure 10).

Furthermore, the main-chain asphericity $A_{mc}$, representing the overall shape of the main chain, increases monotonously with $\sigma_b$ (Figure 11b), which is in line with the behavior of the main-chain persistence length $l_{p,mc}$ (Figure 11a). However and important to notice, while the brush polymer with few and long side chains $[(m, N_{sc}) = (1, 24)]$ displays the *weakest local stiffness*, this polymer has the *largest extended* main chain. Obviously, the bending characteristic on short and on long length scales depends differently on the distribution of a given number of side chains into few and long vs numerous and short side chains.

The rms radius of gyration (Figure 11c), expressing the spatial extension of the polymer, increases with increasing branching density. At low branching density, the overall size of the branched

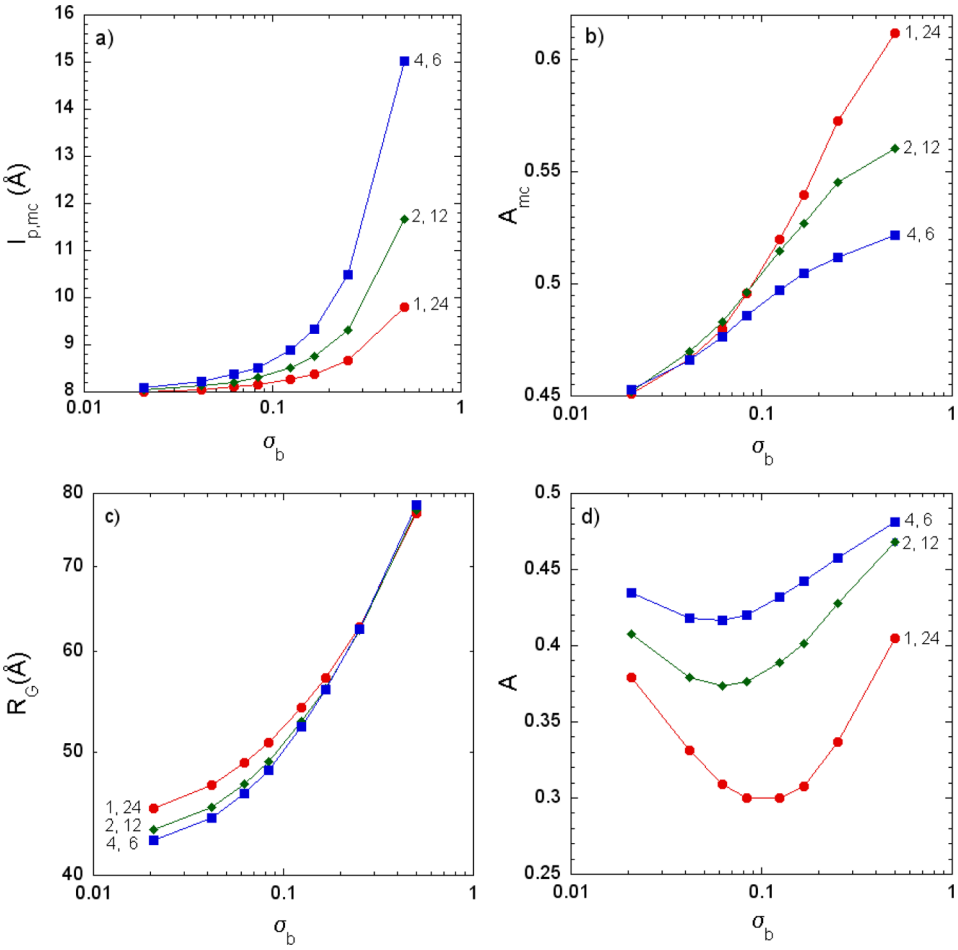


**Figure 11.** (a) Persistence length of the main chain $l_{p,mc}$, (b) asphericity $A_{mc}$ of the main chain, (c) rms radius of gyration $R_G$ of the polymer, and (d) asphericity $A$ of the polymer as a function of branching density $\sigma_b$ for $mN_{sc}$ = 24 beads associated with each node according to $(m, N_{sc}) = (1, 24)$ (●), $(m, N_{sc}) = (2, 12)$ (♦), and $(m, N_{sc}) = (4, 6)$ (■), where $m$ denotes the branching multiplicity and $N_{sc}$ the side-chain length.


dx.doi.org/10.1021/ma4021246 | *Macromolecules* 2014, 47, 415−426

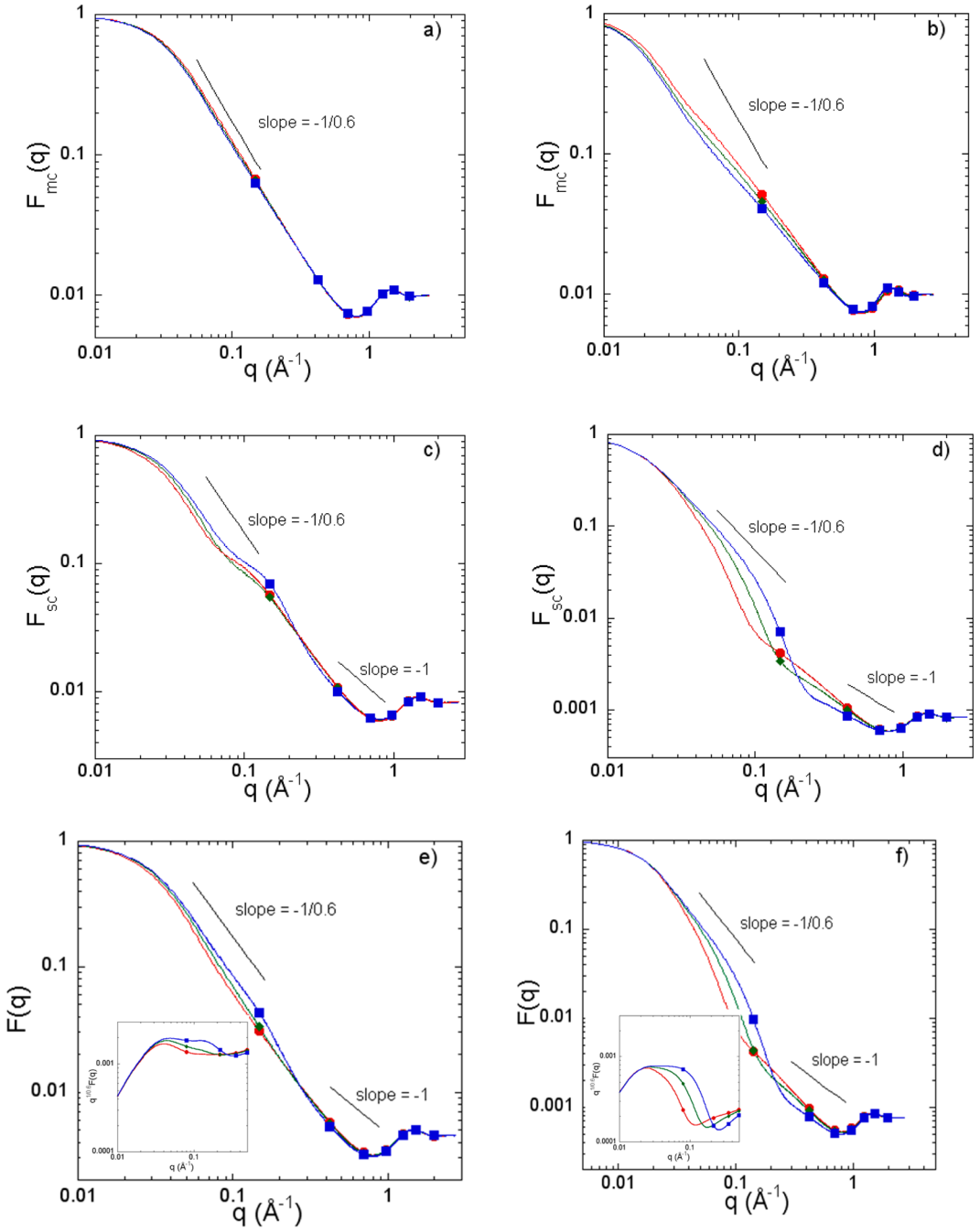


**Figure 12.** (a, b) Main-chain form factor $F_{mc}(q)$, (c, d) side-chain form factor $F_{sc}(q)$, and (e, f) polymer form factor $F(q)$ as a function of the wave vector $q$ in a log−log representation at branching density (a, c, e) $\sigma_b = 0.041$, and (b, d, f) $\sigma_b = 0.50$ for 24 beads associated with each node with side-chain length $(m, N_{sc}) = (1, 24)$ (●), $(m, N_{sc}) = (2, 12)$ (♦), and $(m, N_{sc}) = (4, 6)$ (■), where $m$ denotes the branching multiplicity and $N_{sc}$ the side-chain length. Inserts in the last row display the form factor $F(q)$ in the rescaled form $q^{1/0.6}F(q)$.

polymer is largest with one long side chain per node. However, at $\sigma_b \geq 0.2$, the rms radii of gyration $R_G$ curves superimpose.

As to the asphericity $A$ of the whole polymer, it is sensitive to the value $(m, N_{sc})$, denoting the branching multiplicity and number of beads in a side chain, and to the branching density (Figure 11d). The range of the asphericity values lies between 0.3 and 0.5, and it increases in the order of $(m, N_{sc}) = (1, 24) \rightarrow (2, 12) \rightarrow (4, 6)$ at fixed $\sigma_b$. Noticeably, at all three values of $(m, N_{sc})$ considered, the asphericity displayed a *nonmonotonous* variation as a function of the branching density. Starting from the limit of comb polymers ($\sigma_b = 0.041$), the asphericity $A$ is relatively large and reduces initially at increasing branching density. However, at further increase beyond $\sigma_b \approx 0.1$, $A$ starts to increase.

The simulations with the longer main chain having $N_{mc} = 339$ beads displayed basically the same quantitative persistence-length and $R_G$ scaling behavior, whereas the values of the asphericity were shifted for the three selected values of $\sigma_b$ investigated

*3.2.3. Form Factors.* Finally, we turn to the investigation of the form factor $F(q)$, reporting on the intramolecular correlations, and therefore it provides information on the structure of the scattering object. The form factor is an observable readily measured by light, neutron, or X-ray scattering techniques. Particularly, partial form factors of the main and side chain can be


dx.doi.org/10.1021/ma4021246 | *Macromolecules* 2014, 47, 415−426

obtained separately by selective deuteration of the polymers using small angle neutron scattering (SANS).

Figure 12 depicts the form factor of the main chain $F_{mc}$, side chains $F_{sc}$, and the polymer $F$ normalized such that $F(q) \rightarrow 1$ as $q \rightarrow 0$ as a function of scattering wave vector $q$. We will here examine the cases of the smallest $\sigma_b = 0.041$ and largest $\sigma_b = 0.50$ branching densities with $mN_{sc} = 24$ side-chain beads associated with each node according to $(m, N_{sc}) = (1, 24)$, $(2, 12)$, and $(4, 6)$. Occasionally, we will convert from reciprocal to real space through $r \approx 2\pi/q$.

As to the main-chain form factor $F_{mc}(q)$, in the interval $0.05 < q\text{Å} < 0.5$ $(10 < r\text{Å}^{-1} < 100)$ it is nearly linear in a log−log representation (Figure 12, parts a and b). At $\sigma_b = 0.041$ (Figure 12a), we find $F_{mc}(q) \sim q^{-1/\eta}$ for $0.03 < q\text{Å} < 0.7$ with $\eta = 0.6$ for all three values of $(m, N_{sc})$, which implies that the main chain behaves as a SAW. With increasing grafting density, $F_{mc}(q)$ for different values of $(m, N_{sc})$ splits gently. At $\sigma_b = 0.50$ (Figure 12b), the splitting appears for $0.02 < q\text{Å} < 0.2$. Despite the fact that scattering function still basically behaves as $F_{mc}(q) \sim q^{-1/\eta}$, the exponent deviates from that of a SAW,[38] which indicates a changed shape of the main chain.

As compared to the main chain, the form factors of the side chains are more complex (Figures 12c and 12d). For the different values of $(m, N_{sc})$, we observe a splitting in the range $0.03 < q\text{Å} < 0.1$ at $\sigma_b = 0.041$ (Figure 12c) and a larger one in the range $0.03 < q\text{Å} < 0.6$ at $\sigma_b = 0.50$ (Figure 12d). Obviously, the side chain structure is more affected than the main-chain structure by variation of the topological location of the side-chain beads.

Finally, the polymer form factor $F_{mc}(q)$ (Figure 12, parts e and f) falls in between. To visually enhance features beside SAW chain statistics, we multiply $F(q)$ with $1/q^{-1/\eta}$, $\eta = 0.6$, where $q^{-1/\eta}$ is the form factor of a SAW. In this representation, we observe (i) a splitting in the range $0.03 < q\text{Å} < 0.1$ for the different values of $(m, N_{sc})$, (ii) a local minimum at $q = 0.1-0.2$ Å$^{-1}$, which location is sensitive to the value of $(m, N_{sc})$, and (iii) at $q > 0.2$ Å$^{-1}$ the splitting decreases and the slopes get close to unity. Moreover, all form factors display local maxima located at $q \approx 1.4$ Å$^{-1}$. These maxima originate from the spatial correlation of bonded beads, which rms distance is $R_{bb} \approx 5.5$ Å.

As to observation (i), we relate the splitting in the range of $0.03 < q\text{Å} < 0.1$ with different structures on the length scale of ≈60 to 200 Å, which covers the overall shape of the branched polymer. The contribution to the form factor from the side chains increases with branching density, and except for $\sigma_b = 0.041$ it dominates over the contribution from the main chain. This increase in dominance of the scattering from side-chain beads with increasing branching density correlates well with the simultaneous increase in the splitting for different values of $(m, N_{sc})$. We attribute observation (ii) to correlations on the length scale 30−60 Å comparable to the diameter of the cross section of the branched polymer. Moreover, at $\sigma_b = 0.50$ (Figure 12f) the minimum in $F(q)$ shifts to larger $q$-values, and it become sharper in the sequence $(m, N_{sc}) = (1, 24) \rightarrow (2, 12) \rightarrow (4, 6)$, in agreement with the notion that the radius of the dress decreases and the dress becomes denser in the sequence given above. Finally, observation (iii) corresponds to features on an even shorter length scale. The functional form $F(q) = 1/q^{-1/\eta}$ with $\eta = 1$ is expected for a rigid cylinder and $\eta \approx 0.588$ for a SAW. Here, we span $\eta = 0.65-0.75$. The similar slope of the different values of $(m, N_{sc})$ indicates that the bead−bead correlations on length scales of a few bead−bead separations do not differ much between the three different polymers.

## 4. DISCUSSION

**4.1. Grafting vs Branching Density.** Monograft polymers are characterized by having one side chain per node, whereas multigraft polymers have more than one side chain per node. The concept "grafting density" used for monograft polymers needs to be reconsidered when applying it to multigraft polymers. For multigraft polymers, we let (i) *grafting density* denotes the linear density of grafted *side chains*, (ii) whereas *branching density* denotes the linear density of *nodes* along the main chain, at which the side chains are attached to. For monograft polymers, the concepts "grafting density" and "branching density" obviously degenerate.

**4.2. Two Sources of Repulsion Among Side Chains.** A flexible polymer becomes less flexible upon grafting of side chains owing to the steric repulsion among the side chains. In a regularly branched polymer, the length of the side chains and the linear density of grafted chains both influence the increased stiffening of the main chain. Multigraft polymers introduce yet another feature to regulate the side-chain repulsion, i.e., by varying the number of side chains attached to a node. An increase of the number of grafted side chains attached on a node leads to an enhanced local density of side-chain beads, which, in good solvent, raises the steric repulsion among these side chains and results in a local stiffening of the main chain.

In multigraft polymers, it is conceptually useful to divide the steric repulsion among side chains according to the location of the interacting side chains according to

(1) the repulsion among side chains attached on *different* nodes
(2) the repulsion within a set of side chains grafted on *same* node

In point 1, repulsion is only operating when the locations of the two nodes, to which the side chains are attached, are sufficiently close in space. This repulsion is hence dependent on the branching density, as higher branching density makes the dress of side-chain beads thicker. Therefore, there exists a lower branching density, below which the chains grafted on adjacent nodes cease to always repel each other. In point 2, repulsion is always omnipresent, i.e., appears independently of the branching density.

This simplistic notion is supported by Figure 3 and Figure S1 in three aspects:

(i) Simulation results presented in Figure 3a and Figure S1a confirm the existence of a branching density such that $R_{G,sc}$ is independent of $\sigma_b$ for $\sigma_b \leq \sigma_b^* \approx 0.1$. Thus, below $\sigma_b^*$ the spatial extension of the side chains becomes independent of the branching density. Hence, the repulsion between two side-chain coils is only of secondary importance at $\sigma_b < \sigma_b^*$. The value of $R_{G,sc} \approx 15-16$ Å is similar to $R_{BB}(1/\sigma_b)^{0.6} \approx 20$ Å, where $R_{BB} \approx r_0$ has been used, supporting the notion of the appearance of steric repulsion between side chains grafted on adjacent nodes at $\sigma_b > \sigma_b^*$. As indicated above, such a steric repulsion may also appear at $\sigma_b < \sigma_b^*$; however, that becomes dependent on the main-chain configuration. The main chain has to be folded such that the two side chains become close in space.
(ii) For $\sigma_b < \sigma_b^*$, where an steric repulsion among side chains is not operating, Figure 3a and Figure S1a confirm an increased extension of side chains when they are attached on the same node and that this length increase grows as the number of side chains attached on a node is increased. The


dx.doi.org/10.1021/ma4021246 | Macromolecules 2014, 47, 415−426

increase of the side-chain extension is also here interpreted as a response to alleviate the steric repulsion among side chains grafted on same node.

(iii) For $\sigma_b > \sigma_b^*$, the extension of the side chains increases with increasing branching density, i.e., the side chains become more extended as they are attached closer to each other. An anisotropic size increase appears to reduce the steric repulsion among them. Moreover, at sufficiently high branching density, we envision that the steric repulsion arising from interactions 1 and 2 becomes of the same magnitude. At this condition, the extension of the side chains should depend on the *grafting* density $\sigma_g = m\sigma_b$ only, not on the branching multiplicity $m$ or the branching density $\sigma_b$ individually. Figure 3b and Figure S1b demonstrate that this appears for $\sigma_g > m\sigma_b^*$ with $\sigma_b^* \approx 0.1$. At these grafting densities we view the main chain as being dressed with a cylindrical region of side-chain beads and that this region is basically homogeneous along the main chain.

The conceptual division of the steric repulsion is also fruitful for the interpretation of how the extension of the side chains scales with the number of beads in a side chain. Figure 4 showed that the exponent $\nu_{sc}$ is essentially constant up $\sigma_g \approx m\sigma_b^*$and increases for larger $\sigma_g$. The constant values at $\sigma_g < m\sigma_b^*$ are $\nu_{sc} \approx 0.64$ for $R_{G,sc}$ and $\nu_{sc} \approx 0.66$ for $R_{EE,sc}$, and the value at the largest $\sigma_g$ is 0.67 and 0.73, respectively. Thus, when side chains are separated by residing on different nodes, $\nu_{sc}$ becomes larger than $\nu \approx 0.588$ but smaller than the theoretical value $2\nu/(1 + \nu) \approx 0.741$ applicable to bottle brushes.[22]

**4.3. Main-Chain Extension and Scaling.** The dependence of the main-chain extension and its scaling dependence on the side-chain length $N_{sc}$ and grafting density $\sigma_g$ display noticeable simplification when viewed in reduced parameters. Figure 7 and Figure S5 demonstrate a universal behavior for the reduced rms radius of gyration $R_{G,mc}(N_{sc})/R_{G,mc}(N_{sc} = 0)$ as a function of $\sigma_g^{\mu_{sc}}N_{sc}^{\mu_{sc}}$ where $\mu_{sc}$ is independent of $m$ and $\sigma_g$ (Figure 6a and Figure S4a) and $\nu_{sc}$ is dependent on $m$ and $\sigma_g$.

We have so far discussed results obtained through varying the branching multiplicity under constant length of a side chain (case labeled A in the Introduction). Now we will consider polymer properties under simultaneous variation of the branching multiplicity $m$ and the length of a side chain $N_{sc}$, such that the number of side-chain beads associated with a node $mN_{sc}$ is constant (case labeled B in the Introduction). In other words, how does a redistribution from, say, few long side chains to several shorter ones grafted to the same node affect properties of the branched polymer?

The effect of such a redistribution grew with increasing branching density (Figure 11). At the smallest branching density, no signs of an altered main-chain structure were observed for the side-bead redistribution at $mN_{sc}$ constant. Most likely, the branching density $\sigma_b = 0.041$ (corresponding to equal amount of main-chain and side-chain beads) is too small to have *any* sizable influence on the structure of the main chain under the conditions of our study. However, we did find changes of properties of the polymer, such as its rms radius of gyration (Figure 11c) and its asphericity (Figure 11d), and hence those changes arose from a *direct* contribution from the side-chain beads to these properties.

At the highest branching density $\sigma_b = 0.50$, the situation is less trivial. Changes of polymer properties occurred both (i) from a direct contribution of the redistribution of the side-chain beads and (ii) through an indirect mechanism involving a change of the main-chain structure. With a few and long side chains, the main chain is only moderately stiffened on a short-range scale (Figure 11a), whereas the directional main-chain correlation remains even on a long-range scale (Figure 11b). However, with a larger number of shorter side chains, the main-chain becomes stiffer on the short-range scale (cf. curves labeled by squares and circles in Figure 11a), and less stiff on the long-range scale (cf. curves labeled by squares and circles in Figure 11b).

Peculiar bending properties of branched polymers has earlier been discussed in the literature.[8] Particularly, the usefulness of the concept persistence length has been challenged. The main reason is the existence of more than one length scale with different bending properties. Here, we observe how bending properties at two different length scales are differently affected by the redistribution of side-chain beads considered; the short-range bending resistance is decreased and the long-range bending resistance is increased.

## 5. CONCLUSIONS

A systematic simulation investigation of equilibrium structures of multigraft polymers using a coarse-grained bead−spring model has been performed. The flexible side chains were attached to nodes residing in the main chain. We have considered the cases of one, two, and four side chains at (A) fixed side-chain length and (B) fixed number of side-chain beads associated with a node. Throughout, the fraction of main-chain beads carrying side chains have been varied from ≈0.02, corresponding to the comb−polymer regime, to 0.5, corresponding to the brush-polymer regime. All beads were considered to be in a good solvent.

One particular outcome of this contribution is the need to discriminate between linear branching density and the linear grafting density. The former refers to the density of nodes and the latter the density of side chains, these two quantities not being equal for multigraft polymers.

Moreover, we have also found that the variation of side-chain conformations are mainly controlled by excluded volume interactions between side chains attached to the successive nodes, whereas the interaction among side chains attached to the same node is to the leading order independent of the branching density. The main-chain conformation, however, was controlled by the total number of grafted side chains and not on the individual values of the branching density and branching multiplicity.

Multigraft polymers with equal number of side-chain beads but unequal numbers and lengths of side chains displayed unconventional main-chain bending properties. Few and long side chains gave rise to a still relative low locally stiffness but considerable long-range rigidity, whereas more numerous and shorter side chains lead to a higher local stiffness but to a smaller long-range rigidity. The overall polymer became more spherical-like with few and long side chains, whereas its overall size as measured by the radius of by gyration was only weakly dependent upon the division into side-chain length and number of side chains.

Finally, our study revealed that the scaling formalism employed for describing comb polymers also is useful for describing scaling properties of multigraft polymers or their different subchains at all branching densities and at all branching multiplicity studied. The evidence were obtained by adequate descriptions in terms of power-law dependences found for the radius of gyration and the end-to-end distances of the polymers or their subchains.


dx.doi.org/10.1021/ma4021246 | *Macromolecules* 2014, 47, 415−426

## ■ ASSOCIATED CONTENT

### Supporting Information

Graphical data on the end-to-end distance corresponding to those of the radius of gyration presented in Figures 3, 4, 6, 7, and 8 as well as selected data of fits to eq 14. This material is available free of charge via the Internet at http://pubs.acs.org.

## ■ AUTHOR INFORMATION


### Corresponding Author

*E-mail: (D.G.A.) dangelescu@hotmail.com.


### Notes

The authors declare no competing financial interest.

## ■ ACKNOWLEDGMENTS

This work was supported by a grant of the Romanian National Authority for Scientific Research, CNCS−UEFISCDI, Project Number PN-II-RU-TE-2012-3-0036. D.G.A. espresses thanks for the use of the HPC facilities developed under NASR Grant, Capacities Project CpI 84/2007. Financial support by the Swedish Research Council (VR) through the Linnaeus grants for the Organizing Molecular Matter (OMM) Center of Excellence (239-2009-6794) and through an individual grant to P.L. (2010-2253-78321-47) is gratefully acknowledged.

## ■ REFERENCES


(1) Zhang, M.; Muller, A. H. E. *J. Polym. Sci., Part A: Polym. Chem.* **2005**, *43*, 3461−3481.
(2) Bhattacharya, A.; Misra, B. N. *Prog. Polym. Sci.* **2004**, *29*, 767−814.
(3) Potemkin, I. I.; Palyulin, V. V. *Polym. Sci., Ser. A* **2009**, *51*, 123−149.
(4) Sheiko, S. S.; Sumerlin, B. S.; Matyjaszewski, K. *Prog. Polym. Sci.* **2008**, *33*, 759−785.
(5) Subbotin, A. V.; Semenov, A. N. *Poly. Sci., Ser. A* **2007**, *49*, 1328−1357.
(6) Hadjichristidis, N.; Pitsikalis, M.; Iatrou, H.; Driva, P.; Chatzichristidi, M.; Sakellariou, G.; Lohse, D. Graft copolymers. In *Encyclopedia of Polymer Science and Technology*; Seidel, A., Ed. John Wiley: New York, 2010.
(7) Breitenkamp, R. B.; Emrick, T. *Biomacromolecules* **2008**, *9*, 2495−2500.
(8) Hsu, H.-P.; Paul, W.; Binder, K. *Macromol. Theory Simul.* **2011**, *20*, 510−525.
(9) Rouault, Y.; Borisov, O. V. *Macromolecules* **1996**, *29*, 2605−2611.
(10) Rouault, Y. *Macromol. Theory Simul.* **1998**, *7*, 359−365.
(11) Elli, S.; Ganazzoli, F.; Timoshenko, E. G.; Kuznetsov, Y. A.; Connolly, R. *J. Chem. Phys.* **2004**, *120*, 6257−6267.
(12) Yethiraj, A. *J. Chem. Phys.* **2006**, *125*, 204901.
(13) Khalatur, P. G.; Shirvanyanz, D. G.; Starovoitova, N. Y.; Khokhlov, A. R. *Macromol. Theory Simul.* **2000**, *9*, 141−155.
(14) Connolly, R.; Bellesia, G.; Timoshenko, E. G.; Kuznetsov, Y. A.; Elli, S.; Ganazzoli, F. *Macromolecules* **2005**, *38*, 5288−5299.
(15) Theodorakis, P. E.; Hsu, H.-P.; Paul, W.; Binder, K. *J. Chem. Phys.* **2011**, *135*, 164903.
(16) Hsu, H.-P.; Paul, W.; Binder, K. *J. Chem. Phys.* **2010**, *133*, 134902.
(17) Hsu, H.-P. *Phys. Proc.* **2011**, *15*, 44−53.
(18) Saariaho, M.; Ikkala, O.; Szleifer, I.; Erukhimovich, I.; ten Brinke, G. *J. Chem. Phys.* **1997**, *107*, 3267−3276.
(19) Hsu, H.-P.; Binder, K. *J. Chem. Phys.* **2012**, *136*, 024901.
(20) Sheng, Y.-J. *J. Chem. Phys.* **2004**, *121*, 1962.
(21) Saariaho, M.; Subbotin, A.; Szleifer, I.; Ikkala, O.; ten Brinke, G. *Macromolecules* **1999**, *32*, 4439−4443.
(22) Hsu, H.-P.; Paul, W.; Binder, K. *Macromol. Theory Simul.* **2007**, *16*, 660−689.
(23) Shiokawa, K.; Itoh, K.; Nemoto, N. *J. Chem. Phys.* **1999**, *111*, 8165−8173.
(24) Subbotin, A.; Saariaho, M.; Ikkala, O.; ten Brinke, G. *Macromolecules* **2000**, *33*, 3447−3452.
(25) Subbotin, A.; Saariaho, M.; Stepanyan, R.; Ikkala, O.; ten Brinke, G. *Macromolecules* **2000**, *33*, 6168−6173.
(26) Gu, L.; Shen, Z.; Zhang, S.; Lu, G.; Zhang, X.; Huang, X. *Macromolecules* **2007**, *40*, 4486−4493.
(27) Plamper, F. A.; Reinicke, S.; Elomaa, M.; Schmalz, H.; Tenhu, H. *Macromolecules* **2010**, *43*, 2190−2203.
(28) Yuan, Y.-Y.; Du, Q.; Wang, Y.-C.; Wang, J. *Macromolecules* **2010**, *43*, 1739−1746.
(29) Schlegel, R.; Duan, Y. X.; Weidisch, R.; Hölzer, S.; Schneider, K.; Stamm, M.; Uhrig, D.; Mays, J. W.; Heinrich, G.; Hadjichristidis, N. *Macromolecules* **2011**, *44*, 9374−9383.
(30) Uhrig, D.; Mays, J. *Polym. Chem.* **2011**, *2*, 69−76.
(31) Uhrig, D.; Schlegel, R.; Weidisch, R.; Mays, J. *Eur. Polym. J.* **2011**, *47*, 560−568.
(32) Mijovic, J.; Sun, M.; Pejanovic, S.; Mays, J. M. *Macromolecules* **2003**, *36*, 7640−7651.
(33) Uhrig, D.; Mays, J. W. *Macromolecules* **2002**, *35*, 7182−7190.
(34) Akinchina, A.; Linse, P. *Macromolecules* **2002**, *35*, 5183−5193.
(35) Linse, P. *MOLSIM 5.5.1 ver*; Lund University: Lund, Sweden, 2013.
(36) Muthukumar, M.; Nickel, B. G. *J. Chem. Phys.* **1987**, *86*, 460.
(37) Birshtein, T. M.; Borisov, O. V.; Zhulina, Ye.B.; Khokhlov, A. R.; Yurasova, T. A. *Polym. Sci. U.S.S.R.* **1987**, *29*, 1293−1300.
(38) Rathgeber, S.; Pakula, T.; Wilk, A.; Matyjaszewski, K.; Beers, K. L. *J. Chem. Phys.* **2005**, *122*, 124904.
(39) Rathgeber, S.; Pakula, T.; Wilk, A.; Matyjaszewski, K.; Lee, H.-i.; Beers, K. L. *Polymer* **2006**, *47*, 7318−7327.
(40) Zhang, B.; Gröhn, F.; Pedersen, J. S.; Fischer, K.; Schmidt, M. *Macromolecules* **2006**, *39*, 8440−8450.
(41) Terao, K.; Nakamura, Y.; Norisuye, T. *Macromolecules* **1999**, *32*, 711−716.
(42) Fischer, K.; Schmidt, M. *Macromol. Rapid Commun.* **2001**, *22*, 787−791.
(43) Halperin, A.; Tirrell, M.; Lodge, T. Tethered Chains in Polymer Microstructures. In *Advances in Polymer Science*; Springer: Berlin, 1992; Vol. *100*, pp 31−71.
(44) Wintermantel, M.; Gerle, M.; Fischer, K.; Schmidt, M.; Wataoka, I.; Urakawa, H.; Kajiwara, K.; Tsukahara, Y. *Macromolecules* **1996**, *29*, 978−983.
(45) Fredrickson, G. H. *Macromolecules* **1993**, *26*, 2825−2831.